BBA - General Subjects 1862 (2018) 1168–1179

Contents lists available at ScienceDirect

BBA - General Subjects

journal homepage: www.elsevier.com/locate/bbagen

Iron transport kinetics through blood-brain barrier endothelial cells

Aminul Islam Khan, Jin Liu, Prashanta Dutta*

School of Mechanical and Materials Engineering, Washington State University, Pullman, WA 99164-2920, United States

ARTICLE INFO

Keywords:
Blood-brain barrier
Apo-transferrin
Holo-transferrin
Transferrin receptors

ABSTRACT

Background: Transferrin and its receptors play an important role during the uptake and transcytosis of iron through blood-brain barrier (BBB) endothelial cells (ECs) to maintain iron homeostasis in BBB endothelium and brain. Any disruptions in the cell environment may change the distribution of transferrin receptors on the cell surface, which eventually alter the homeostasis and initiate neurodegenerative disorders. In this paper, we developed a comprehensive mathematical model that considers the necessary kinetics for holo-transferrin internalization and acidification, apo-transferrin recycling, and exocytosis of free iron and transferrin-bound iron through basolateral side of BBB ECs.

Methods: Ordinary differential equations are formulated based on the first order reaction kinetics to model the iron transport considering their interactions with transferrin and transferrin receptors. Unknown kinetics rate constants are determined from experimental data by applying a non-linear optimization technique.

Results: Using the estimated kinetic rate constants, the presented model can effectively reproduce the experimental data of iron transports through BBB ECs for many in-vitro studies. Model results also suggest that the BBB ECs can regulate the extent of the two possible iron transport pathways (free and transferrin-bound iron) by controlling the receptor expression, internalization of holo-transferrin-receptor complexes and acidification of holo-transferrin inside the cell endosomes.

Conclusion: The comprehensive mathematical model described here can predict the iron transport through BBB ECs considering various possible routes from blood side to brain side. The model can also predict the transferrin and iron transport behavior in iron-enriched and iron-depleted cells, which has not been addressed in previous work.

1. Introduction

The central nervous system is protected by three principal barrier sites at the interface between blood vessel and brain tissue: the blood-brain barrier (BBB), blood-cerebrospinal fluid barrier and the arachnoid barrier [1]. Among them, the BBB ensures the safety and proper functioning of brain by regulating the penetration of different nutrients/molecules from blood to brain and vice versa. This dynamic and highly selective membrane prohibits the direct contact of circulating blood with the brain extracellular fluid in the central nervous system and protects the brain against invading organisms and unwanted substances [2]. The BBB is comprised of brain endothelial cells, which are connected by tight junctions [3] and adherens junctions [4]. Although all blood capillaries are separated from surrounding tissue by endothelial cells, the tight junctions between endothelial cells are only present in brain-blood capillaries [5]. These tight junctions are facilitated by different transmembrane and cytoplasmic proteins [2,6], and have the capability to restrict paracellular diffusion of water-soluble substances from luminal (apical) side to the abluminal (basolateral) side of BBB [7]. Moreover, the BBB endothelial cells do not provide any direct passageways such as fenestrations or channels, and have the minimal rate of pinocytosis for large lipophilic compounds [6]. These properties make the BBB highly selective to transport of biologics from cerebral capillaries to the brain parenchyma and vice versa.

Although the BBB tight junction helps to protect the brain from unnecessary intrusions, it makes the drug delivery across the BBB extremely challenging for treatment of brain diseases. As a result, the treatment of many neurodegenerative disorders is still ineffective, even though many potential drugs were screened out. One potential solution is to understand the transport mechanism of nutrients, such as iron, insulin, caffeine etc. across the BBB, and then mimic the mechanism for drug. Moreover, understanding the details of nutrient transport across BBB would help to prevent some neurodegenerative disorders like Alzheimer's and Parkinson's diseases.

Iron is a crucial element for fundamental metabolic processes of brain cells. Iron can serve as an electron acceptor and donor, which

* Corresponding author.
E-mail address: prashanta@wsu.edu (P. Dutta).

https://doi.org/10.1016/j.bbagen.2018.02.010
Received 24 January 2018; Accepted 14 February 2018
Available online 18 February 2018

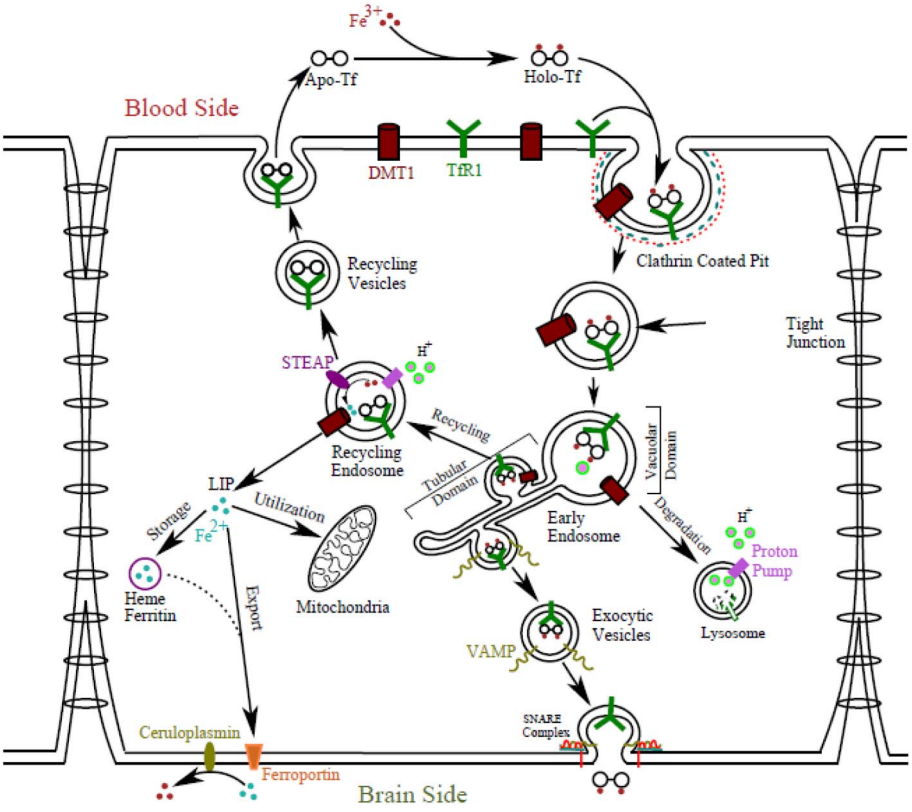

Fig. 1. Iron transport through transferrin receptor-mediated pathway across BBB endothelium.

makes it vital for various physiological and metabolic processes such as oxygen transport in the cell and energy production in mitochondria. However, a change in iron concentration may cause malfunctions in important organs such as liver and brain. For instance, in case of Parkinson's, Alzheimer's and some other neurodegenerative disorders, an abnormally high level of irons has been reported in the brain [8–10]. On the other hand, millions of people are affected by so called anemia due to a significant deficiency of irons. Therefore, to maintain the homeostasis, the transport of iron across BBB and the iron level in the brain parenchyma must be properly regulated.

It has been reported that irons are primarily transported through cells via transferrin regulated processes. The receptors for transferrin regulated transport were discovered in the middle of 20th century for red blood cells [11]. Later it was found that many other types of cells also use these receptors for iron transport, and subsequently, the receptors were named as transferrin receptors [12–15]. For BBB endothelial cells, the transferrin receptors were first identified by Jefferies et al. [16] in 1984. They hypothesized that the transferrin receptors are expressed on brain endothelium to facilitate the transport of transferrins and thus irons into the brain. After their initial findings, numerous experimental works were undertaken to address the iron transport mechanism in BBB endothelial cells [17–23]. These works have established that the brain derive its irons by the receptor-mediated transport of holo-transferrin through the brain capillary endothelium, although there are some debates on the exact pathway [24]. The first receptor-mediated transport of iron across the BBB was examined by Fishman et al. [17] with rat brain. Later, this receptor-mediated transcytosis was further validated by Raub and Newton [19], Descamps et al. [21] and Burdo et al. [22] with bovine brain and retinal endothelial cells.

During the receptor-mediated transcytosis, irons transport unidirectionally from blood to brain, while transferrin can follow two routes: recycling to blood or transport to brain [18]. Burdo et al. [22] demonstrated that the transport of irons from blood to brain can occur in two forms: as free irons and transferrin bound irons. They have hypothesized that the free irons come from the acidification of holo-transferrin in the endosome.

Although there are numerous experimental works on iron transport through different kind of cells, only a few theoretical works addressed the transferrin kinetics during iron transport into brain or other cells. This is, perhaps, due to the lack of information about the endocytosis and exocytosis mechanisms of iron-loaded ligand-receptor complex. Ciechanover et al. [25] experimentally determined a few parameters such as the rate of internalization, the rate of association and dissociation etc. for transferrin kinetics in human hepatoma cell, and proposed a mathematical model based on these parameters to study internalization and recycling of transferrin and transferrin receptors following the laws of mass action. Later, many researchers have worked on the transferrin kinetics with different kinds of cell lines, such as isolated rabbit reticulocytes [26], epidermoid carcinoma cells [27], Madin-Derby canine kidney epithelial cells [28] to determine the transferrin kinetics parameters experimentally. Mayle et al. [29] reviewed the parameter determination procedures and proposed an intracellular trafficking pathway of transferrin for a general cell, in which only transferrin endocytosis and recycling exist. However, in case of BBB endothelial cells, this pathway is not appropriate because these cells need irons for their own metabolism processes and, at the same time, they must supply irons to the brain side to meet iron requirements of neuron and other brain cells for proper functioning of brain [30]. *To date, no mathematical model exists for the transcytosis of iron and transferrin though BBB endothelium.*

In this study, a comprehensive mathematical model is proposed for transferrin transcytosis and iron transport through BBB endothelial cells. The rest of the paper is organized as follows. In following section, we present the overall transport process for iron and transferrin through the BBB endothelium. Next, mathematical models are formulated based on mass-action laws for iron uptake, endosomal dissociation, and exocytosis of free and transferrin-bound irons. In Section 4, a non-linear optimization technique is used for finding kinetic parameters for iron,

transferrin and transferrin receptor complexes. Next, we validate the proposed model using the estimated kinetic rate parameters. We then investigate the effect of transferrin concentration in the apical side on iron transcytosis considering the normal operating condition in the cell. Finally, we extend the developed model to investigate iron transport from the apical side to the basolateral side for the iron-enriched and iron-depleted endothelial cells.

2. Overall transport system

In literature, there are different opinions on iron transport through BBB endothelial cells. Some researchers [20,31] found in experiments that irons can only cross BBB endothelial cells as ions. While others experimentally demonstrated that irons can be transported through the basolateral membrane as bounded with transferrin, as well as free irons [22,32,33]. Radiolabeling of transferrin with ^{59}Fe demonstrated that transferrin bound irons can cross the BBB endothelial cells [21]. Here we consider all possible pathways for iron transport though BBB endothelial cells as shown in Fig. 1.

Transferrin receptors are transmembrane glycoproteins having two homologs: transferrin receptor 1 and transferrin receptor 2. Transferrin receptor 1 is a ubiquitously expressed receptor, and their expression on the cerebral capillary surface is regulated by the intracellular iron concentrations. On the other hand, the expression of transferrin receptor 2 is restricted to certain cell types such as liver, small intestine, and their expression is unaffected by the intracellular iron concentrations. Thus, throughout this work, only transferrin receptor 1 is considered since there is no evidence of transferrin receptor 2 expression on the endothelial cell surface [34,35].

Transferrin, an iron-binding protein, has a high binding affinity to the transferrin receptor (K_d = 1–110 nM). The binding affinity of transferrin largely depends on its association with ferrous or ferric iron and pH of the medium [36]. Iron-loaded transferrin (holo-transferrin) binds with transferrin receptor at pH 7.0 [36]. It has been well established that once a holo-transferrin binds with the transferrin receptors on the endothelial cells surface at the apical side, the holo-transferrin-receptor (HTR) complex is internalized into endothelial cells by clathrin-mediated endocytosis [37] as shown in Fig. 1. After the endocytosis, vesicles are trafficked and directed to early or sorting endosome where they are fused with early endosome. Once vesicles reach to the early endosome, the acidification of early endosome occurs by proton pumps and ferric irons are released from the HTR in an acidic pH 5–6 [38]. The released ferric irons are then reduced by the STEAP (six-transmembrane epithelial antigen of the prostate) and transported to the cytosol labile iron pool (LIP) by the divalent metal transporter 1 (DMT1) [39].

LIP is the main compartment for iron and iron-containing compounds' metabolic pathway, and it reduces the availability of free iron inside the cells. From LIP, some irons are used by mitochondria and other organelles, some are stored inside the endothelial cells as hemeferritin, and the others are exported to the brain side by ferroportin [40]. At the acidified endosome (pH 5–6), apo-transferrins (transferrins without irons) bind with transferrin receptors tightly. These apo-transferrins are recycled back to the cell surface following either a fast route (directly from endosome to cell membrane), or a slower route where apo-transferrin-receptor complexes first go to recycling endosome and then to the cell membrane [41]. Cargoes intended for degradation reside in the vacuolar domains of the acidified endosome and continue through the endosome-lysosome maturation process, and finally, degrade in the lysosome. On the other hand, cargoes containing intact holo-transferrin-receptor complex reside in the tubular domains of early endosome, and eventually are directed to the abluminal side of endothelial cells through recycling endosome [42]. Similar to synaptic vesicle exocytosis in neuron, the exocytosis of vesicular carriers in endothelial cells involves soluble NSF (*N*-ethylmaleimide-sensitive factor) attachment protein receptor (SNARE) proteins [43]. The proposed iron pathways contain iron transport mechanisms across the basolateral membrane considering both free iron and holo-transferrin, which will be useful to test the competing hypotheses provided by experimental studies.

3. Mathematical modeling

The endocytosis of transferrin-bound iron into the endothelial cell and the exocytosis through the basolateral membrane involves highly complex biochemical and biophysical processes. These complex processes are dictated by various events, such as expression of receptors on the endothelial cell surfaces, binding of receptors with ligands, membrane deformation, protein-protein and protein-lipid interaction for membrane fusion, etc. which are occurring at multiple time scales. So, it is not possible to include all the details of transport mechanism in the mass-action based mathematical modeling. However, all the important steps of iron transport and transferrin kinetics across the BBB are considered in this model.

3.1. Biological processes involved in iron transport

The overall process of iron transport through endothelial cell is shown in Fig. 2, where the biological processes are separated into four sub-categories: Uptake/endocytosis of holo-transferrin by endothelial cells, dissociation of iron from holo-transferrin-receptor complex and transferrin recycling, exocytosis of free (non-transferrin-bound) iron, and exocytosis of transferrin-bound iron.

3.1.1. Uptake/endocytosis of holo-transferrin by endothelial cells

The cellular uptake of irons is initiated with the binding of ferric irons to transferrins in the circulatory (blood) system. It has been found

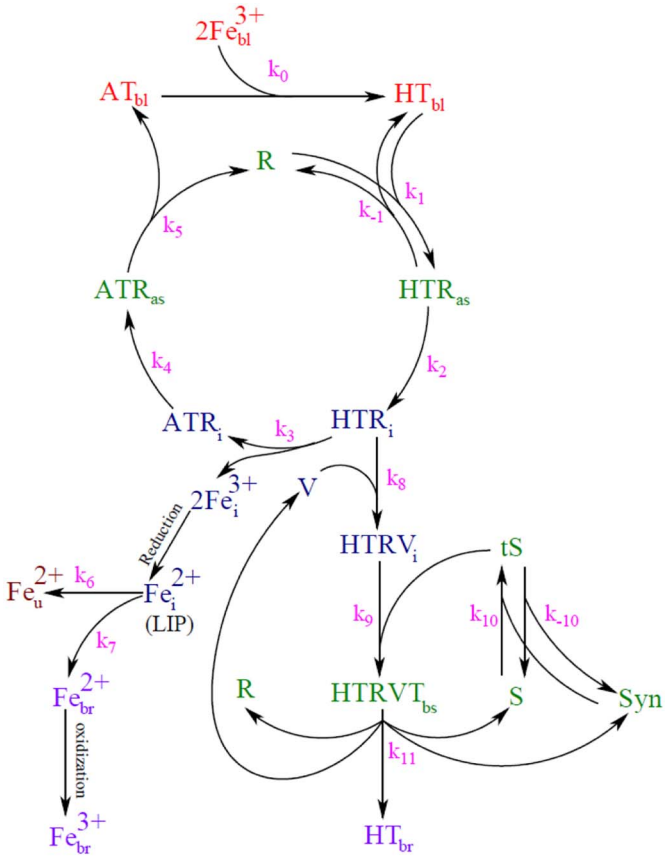

Fig. 2. The overall modeling scheme depicting the essential pathways and parameters for the receptor-mediated transcytosis of iron across the BBB endothelial cells.

that one transferrin can bind with two molecules of ferric iron, Fe^{3+}, to form diferric-transferrin (aka holo-transferrin) as

$$AT_{bl} + 2Fe_{bl}^{3+} \xrightarrow{k_0} HT_{bl} \quad (1)$$

where k_0 is the association rate constant of apo-transferrin (AT) and Fe^{3+}; the subscript bl stands for blood side. The holo-transferrins binds specifically with the transferrin receptors on the apical surface (as) of the endothelial cells. The binding of holo-transferrins to surface receptor can be presented as

$$HT_{bl} + R \underset{k_{-1}}{\overset{k_1}{\longleftrightarrow}} HTR_{as} \quad (2)$$

This is a bi-directional process, where the hollo-transferrin-receptor (HTR) complex is formed on the apical surface. Next the HTR complex is internalized (i) into the cell with the help of clathrin, adapter protein 2, and dynamin

$$HTR_{as} \xrightarrow{k_2} HTR_i \quad (3)$$

Throughout the manuscript, k with positive and negative subscripts represent forward and backward rate constants, respectively.

3.1.2. Dissociation of iron from holo-transferrin-receptor complex and transferrin recycling

After the internalization, clathrin coats dissociate from vesicles due to interaction between hsc protein family and clathrin [44]. Vesicles are then directed to early endosome, where some of them are acidified and ferric irons are released from the HTR_i complex as

$$HTR_i \xrightarrow{k_3} ATR_i + Fe_i^{3+} \quad (4)$$

Then the ATR_i (apo-transferrin-receptor) complex recycles back to apical surface,

$$ATR_i \xrightarrow{k_4} ATR_{as} \quad (5)$$

and subsequently dissociates from the transferrin receptors as

$$ATR_{as} \xrightarrow{k_5} AT + R \quad (6)$$

This apo-transferrin (AT) is now ready to bind with ferric irons to form new holo-transferrin, while the transferrin receptor returns to the apical surface and is available to bind with holo-transferrin. This completes the transferrin recycling process.

The irons released inside the endosome (see Eq. (4)) eventually reach the labile iron pool (LIP) in the cytosol by crossing endosome membrane through DMT1. But, before crossing the endosomal membrane, the ferric irons are reduced by the STEAP protein, a metal reductase, as.

$$Fe_i^{3+} \xrightarrow{\text{reduction}} Fe_i^{2+} \quad (7)$$

In our model, we assume that all the ferric iron reduces to ferrous iron before crossing the endosomal membrane.

3.1.3. Exocytosis of non-transferrin-bound iron

As stated earlier, labile iron pool acts as a source for cellular iron uptake, usage, storage, and export. Based on the demand of energy production, some irons are used by mitochondria and other organelles in the endothelial cell as,

$$Fe_i^{2+} \xrightarrow{k_6} Fe_u^{2+} \quad (8)$$

Some are usually stored by the cells if there is no immediate usage [45], while the rest are exported across the basolateral membrane through ferroportin for brain cells. It has been reported that at the time of crossing the basolateral membrane, these irons are oxidized from ferrous to ferric form by ceruloplasmin for brain use.

$$Fe_i^{2+} \xrightarrow{k_7} Fe_{br}^{2+} \quad (9)$$

$$Fe_{br}^{2+} \xrightarrow{\text{oxidization}} Fe_{br}^{3+} \quad (10)$$

3.1.4. Exocytosis of transferrin-bound iron

It has been well established that SNARE proteins are the main elements responsible for the membrane fusion in different kinds of cells [46,47]. Three SNARE proteins have been identified for docking and fusion of vesicles with the target compartment: vesicle-associated membrane proteins, synaptosomal-associated proteins and plasma membrane proteins (Syntaxin). Different homologs of these proteins are responsible for vesicle secretion in different kind of cells. In case of endothelial cells, SNAP23, Syntaxin 3 or 4 and VAMP 3 or 8 regulate the docking and membrane fusion [43,48,49]. However, residency of Syntaxin 3 is restricted to apical membrane, whereas residency of Syntaxin 4 is limited to basolateral membrane [50]. Thus, Syntaxin 3 is responsible for recycling through apical membrane and Syntaxin 4 is involved in exocytosis through basolateral membrane. In an experimental study, Pulido et al. [47] found that VAMP 8 did not form stable ternary complex with SNAP 23 and Syntaxin 4, whereas VAMP 3 were able to form stable ternary complex during membrane fusion. Thus, their results suggest that the endothelial cells select VAMP 3 over VAMP 8 to interact with SNAP 23 and Syntaxin 4 during exocytosis. Therefore, in our model we assume that the hollo-transferrin bound vesicles attach to VAMP 3 while escaping from the endosomal compartment as

$$HTR_i + V \xrightarrow{k_8} HTRV_i \quad (11)$$

Later these vesicles are trafficked towards basolateral surface (bs) where they interact with target SNARE (t-SNARE) and form the full SNARE complex as

$$HTRV_i + tS \xrightarrow{k_9} HTRVT_{bs} \quad (12)$$

The t-SNARE is synthesized from the interactions between SNAP23 and Syntaxin 4 proteins as

$$S + Syn \underset{k_{-10}}{\overset{k_{10}}{\longleftrightarrow}} tS \quad (13)$$

The assembly of the full SNARE complex (HTRVT) brings the vesicle and basolateral membrane close to each other and open the fusion pores. During the fusion process, holo-transferrins are released from the vesicle into the brain side (Fig. 1), and all other associated proteins are directed to their respective positions.

$$HTRVT_{bs} \xrightarrow{k_{11}} HT_{br} + Syn + S + R + V \quad (14)$$

This fusion process is catalyzed by some other regulatory proteins such as NSF, small GTPase Rab27a, Slp4a (effector of GTPase rab27a), Syntaxin binding proteins (STXBP1 and 5), MyRIP, UNC13 in an undetermined way [48]. In our model, effects of these proteins are accounted for via the fusion rate constant k_{11}. Moreover, in our model, it is assumed that as much receptors released on the basolateral surface are available on the apical membrane. In other words, there is no generation or degradation of transferrin receptors.

3.2. Conversion of biochemical equations into differential equations

To model all the processes listed in Eqs. (1)–(14), we develop a system of ODEs based on the law of mass action:

$$\frac{d[HT_{bl}]}{dt} = k_0[AT_{bl}][Fe_{bl}^{3+}] - k_1[HT_{bl}][R] + k_{-1}[HTR_{as}] \quad (15.1)$$

$$\frac{d[R]}{dt} = -k_1[R][HT_{bl}] + k_{-1}[HTR_{as}] + k_5[ATR_{as}] + k_{11}[HTRVT_{bs}] \quad (15.2)$$

$$\frac{d[HTR_{as}]}{dt} = k_1[R][HT_{bl}] - k_{-1}[HTR_{as}] - k_2[HTR_{as}] \quad (15.3)$$

$$\frac{d[HTR_i]}{dt} = k_2[HTR_{as}] - k_3[HTR_i] - k_8[HTR_i][V] \quad (15.4)$$

$$\frac{d[ATR_i]}{dt} = k_3[HTR_i] - k_4[ATR_i] \quad (15.5)$$

$$\frac{d[ATR_{as}]}{dt} = k_4[ATR_i] - k_5[ATR_{as}] \quad (15.6)$$

$$\frac{d[AT_{bl}]}{dt} = k_5[ATR_{as}] - k_0[AT_{bl}][Fe_{bl}^{3+}] \quad (15.7)$$

$$\frac{d[Fe_{bl}^{3+}]}{dt} = -k_0[AT_{bl}][Fe_{bl}^{3+}] \quad (15.8)$$

$$\frac{d[Fe_i^{2+}]}{dt} = k_3[HTR_i] - (k_6 + k_7)[Fe_i^{2+}] \quad (15.9)$$

$$\frac{d[(Fe_u^{2+})]}{dt} = k_6[Fe_i^{2+}] \quad (15.10)$$

$$\frac{d[(Fe_{br}^{3+})]}{dt} = k_7[Fe_i^{2+}] \quad (15.11)$$

$$\frac{d[HTRV_i]}{dt} = k_8[HTR_i][V] - k_9[HTRV_i][tS] \quad (15.12)$$

$$\frac{d[V]}{dt} = -k_8[HTR_i][V] + k_{11}[HTRVT_{bs}] \quad (15.13)$$

$$\frac{d[tS]}{dt} = -k_9[HTRV_i][tS] + k_{10}[S][Syn] - k_{-10}[tS] \quad (15.14)$$

$$\frac{d[HTRVT_{bs}]}{dt} = k_9[HTRV_i][tS] - k_{11}[HTRVT_{bs}] \quad (15.15)$$

$$\frac{d[HT_{br}]}{dt} = k_{11}[HTRVT_{bs}] \quad (15.16)$$

$$\frac{d[S]}{dt} = k_{11}[HTRVT_{bs}] - k_{10}[S][Syn] + k_{-10}[tS] \quad (15.17)$$

$$\frac{d[Syn]}{dt} = k_{11}[HTRVT_{bs}] - k_{10}[S][Syn] + k_{-10}[tS] \quad (15.18)$$

where the notation [·] represents the concentration of species. Symbols used to denote different chemical compounds are given in Table 1.

Table 1
Symbols used for different molecules, ions, proteins and protein complex.

Notation	Description
Fe_{bl}^{3+}	Free ferric ion in blood capillaries
R	Transferrin receptors
AT_{bl}	Iron-free transferrin in blood capillaries
HT_{bl}	Iron-loaded transferrin in brain capillaries
HTR_{as}	Complex of holo-transferrin and transferrin receptor on apical surface
HTR_i	Complex of holo-transferrin and transferrin receptor inside the cell
ATR_i	Complex of apo-transferrin and transferrin receptor inside the cell
ATR_{as}	Complex of apo-transferrin and transferrin receptor on apical surface
Fe_i^{3+}	Ferric ion inside the cell
Fe_i^{2+}	Ferrous ion in labile iron pool
Fe_u^{2+}	Ferrous ion used by cells
Fe_{br}^{2+}	Ferrous ion exported to brain side
Fe_{br}^{3+}	Ferric ion exported to brain side
V	Vesicle associated membrane protein 3 (VAMP3)
$HTRV_i$	Complex of holo-transferrin and transferrin receptor that is attached with VAMP3
tS	t-SNARE, a complex of SNAP23 and Syntaxin 4 proteins
$HTRVT_{bs}$	HTRV protein complex that is bonded with t-SNARE on basolateral surface
HT_{br}	Holo-transferrin in the brain side
S	Synaptosomal associated protein 23 (SNAP23)
Syn	Syntaxin 4

4. Estimation of model parameters

The mathematical model presented in Eqs. (15.1)–(15.18) involves many rate constants, some of which are not readily available in the literature for BBB endothelial cells. There are some inverse techniques [51,52] available in the literature to estimate those parameters, however, these techniques are very computationally involved for cases like this. Moreover, those techniques fail to provide a specific value for any parameter. Rather they provide a very large range for a parameter, which is practically useless. For instance, Chen et al. [53] applied an inverse technique to estimate kinetic parameters for synaptic vesicle exocytosis (based on the work of [51]), but their estimated parameters vary in several orders of magnitude (4.40×10^3~2.30×10^6 $M^{-1}s^{-1}$).

In this work, the unknown parameters are determined by applying a non-linear least square fit [54]. This method requires a range for searching the true value. In our study, this range is first sought for any endothelial cells. If data is not available in the literatures, reported value of that parameter for other type of cells is used. Moreover, if a specific rate constant is not reported for any kind of cells, we either considered a range that is reported for their homologs or determined the maximum and minimum values of that constant using the Debye-Smoluchowski equation as:

$$k_{max} = \frac{4\pi N_{av}}{1000} \sum R_{j,i} \sum D_{j,i} \quad (16a)$$

$$k_{min} = k_{max}/10^4 \quad (16b)$$

where $R_{j,\ i}$ is the radius of encounter in meter, $D_{j,\ i}$ is the diffusion coefficients of the reactants in cm^2/sec and N_{av} is Avogadro number. Next, we present our method for finding the kinetic rate constant from a predetermined range.

Let us consider the binding rate constant of holo-transferrin and transferrin receptors, k_1 which has been reported as low as 1.0×10^6 $M^{-1}min^{-1}$ [55] to as high as 1.0×10^8 $M^{-1}min^{-1}$ [56] for different type of cells. So, we start from lowest value of k_1 which is ~1.0×10^4 $M^{-1}s^{-1}$ and run the model to fit the predicted values with the experimental results by minimizing the squared deviation per experimental point (SD) while keeping other rate parameters as constant at their fixed reported value or at their lowest reported value. The SD is given by the following equation.

$$SD = \left(\sum_0^N (A_{exp} - A_{model})^2 \right) / N \quad (17)$$

where N is the number of experimental data points available for any parameter A, A_{exp} is the experimental value of any parameter at time t, and A_{model} is the value of that parameter predicted by the model at time t. Next, we change its value by a random amount and then recalculate the new squared deviation. If this new squared deviation is less than the previous squared deviation, then the new parameter value is kept. Otherwise, the previous value is used, and we move forward to find another rate constant until all the parameter values are selected. The program searches both upward and downward for more favorable values of those rate parameters by adding and subtracting a differential amount to those rate parameters for minimization of SD. Fig. 3 shows the plot for finding of two rate constants. As seen from Fig. 3a, for $k_1 = 1.7 \times 10^4$ $M^{-1}s^{-1}$ the model predicts the experimental results with minimum SD. Similarly, as shown in Fig. 3b, the minimum SD occurs for $k_2 = 7.5 \times 10^{-3}$ s^{-1}. So, we select these ($k_1 = 1.7 \times 10^4$ $M^{-1}s^{-1}$ and $k_2 = 7.5 \times 10^{-3}$ s^{-1}) rate constants and do the same analysis for all other unknown rate constants. Later this set of data is further refined by a search within a narrow range of one order of magnitude. Here, it is noteworthy to mention that the estimated parameters are not necessarily the unique value, rather they are a possible set of parameters that can reproduce experimental results. Although the method used in this paper is not the best one, it can provide specific values for each unknown parameters. All the rate constants (known and

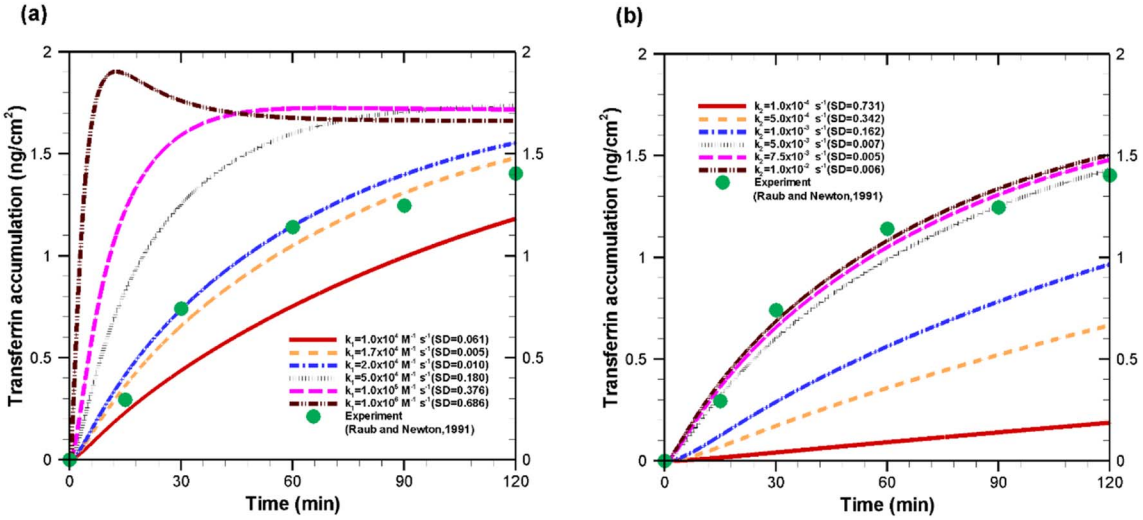

Fig. 3. Calibration curve for a) binding rate constant of holo-transferrin and transferrin receptors, k_1, and b) internalization rate constant of holo-transferrin-receptor complex, k_2. Numerical solutions for different value of k_1 and k_2 are shown as color lines and experimental results from Raub and Newton [19] are shown as green circles. The experiment was performed by culturing the brain microvessel endothelial cells with 10.0 nM of holo-transferrin in the apical side. Similar condition is considered in the numerical simulation to find out the optimized rate constants.

Table 2
Initial conditions for the ODEs system (Eqs. (15.1)–(15.18)).

Protein and protein complex	Value	Reference
HT_{bl}	10 nM–17.5 nM	[19,21]
R	35,000 receptors/cell	[21]
V	10.0 nM	[63]
S	20.0 nM	Calculated from [43][a]
Syn	66.4 nM	Calculated from [64][b]

Note: The initial values of other ions, proteins or protein complexes are considered as zero. Since the developed model is applied for in vitro conditions, this assumption works well for most of the variables. All the calculations are done by considering cell volume equals 3000 μm^3.

[a] The calculation is done by considering 36,000 proteins per cell.

[b] The calculation is done by considering 120,000 proteins per cell.

estimated) used in this analysis are listed in Table 3, while the initial concentrations of required components are provided in Table 2.

5. Results and discussion

5.1. Model validation

We first validate our model and parameters through comparison with experiments. Fig. 4 shows the numerically predicted (solid line) accumulation of transferrin inside the microvessel endothelial cells for different level of initial holo-transferrin concentration on the apical surface. Experimental data (symbol) from Raub and Newton [19] are also presented. In the experiments, cells were grown on matrix-coated plastic, and there was no transport of holo-transferrin to the basolateral side. For transferrin accumulation at different time, cells (at day 6 in culture) were incubated with 10 nM ^{125}I-transferrin at 37 °C and the amount of cell-associated radioactivity were measured. As shown the model results agree well with the experimental data up to 1000 ng/ml of holo-transferrin in the apical side. However, experimental data indicate a saturation of transferrin accumulation above 800 ng/ml (10 nM), which is not reflected in our model result. Later, Descamps et al. [21] did similar experiments with the same brain capillary endothelial cells but no evidence of saturation was found for concentrations of holo-transferrin ranging from 100 to 1400 ng/ml (1.25 to 17.5 nM) in apical side. They argued that the differences were from different experimental protocols. For instance, in the work of Descamps

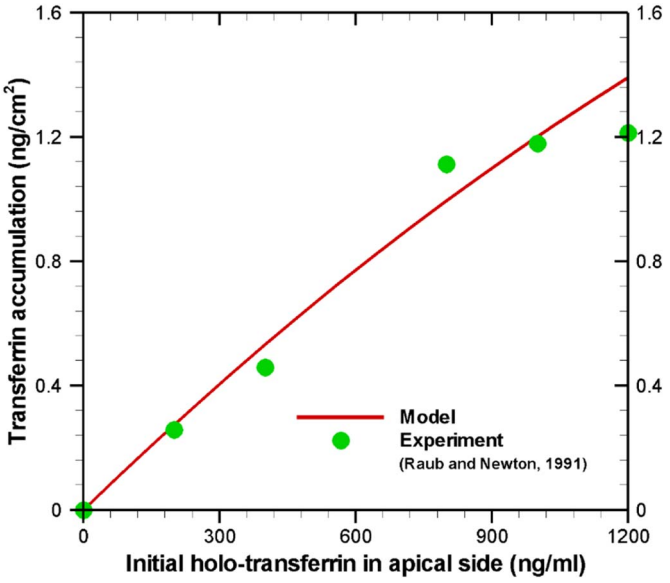

Fig. 4. Accumulation of transferrin inside the brain microvessel endothelial cells for different initial concentration of holo-transferrin at the apical side at 60 mins. Experimental result of Raub and Newton [19] are used for comparison of our model results. The experimental values are converted from ng/dish to ng/cm^2 by dividing the area of dish. For numerical results, the accumulations are converted from ng/ml to ng/cm^2 by considering volume to surface area ratio as 390. Here term 'volume' refers the volume occupied by a single cell and term 'surface area' refers the apical or basolateral surface area of a single cell. It has been reported that volume and surface area of an endothelial cell varies from 1000 to 3000 μm^3 and from 35 to 350 μm^2 [68] respectively. In this study, we have considered the cell volume as 3000 μm^3 and the surface area of a cell is 120 μm^2.

et al., cells were transferred to another well at various time to avoid possible re-endocytosis of transferrin from the abluminal side of the endothelial cells. On the other hand, Raub and Newton [19] did the experiments with continuous incubation. In addition, the cells in Raub and Newton's [19] experiments were grown on a matrix coated plastic, the complete transcytosis was not possible and holo-transferrins accumulated at basolateral membrane. As a result, a large amount of receptors were occupied by the transferrins at basolateral surface and reduced the availability of free receptors at the apical surface for further endocytosis of holo-transferrin.

Another reason for the discrepancy between model prediction and experimental data may be due to the assumption used for the transferrin receptors. In our model, we assume that as much receptors fuses with basolateral membrane during the secretion of holo-transferrin, the same number of receptors are expressed on the apical surface (see Eqs. (13) and (15.2)). This assumption is reasonable if there is substantial recruitment of transferrin receptors from the intracellular pool to the active endocytotic pool as noted by Burdo et al. [22]. But it may not hold in some scenarios. For instance, Visser et al. [57] and Gelder et al. [58] experimentally found that the expression of transferrin receptors on the endothelial cell surface largely depends on the cellular iron concentration. As the intracellular iron concentration increases, the expression of transferrin receptors decreases and vice-versa. Thus, with the uptake of holo-transferrin from apical surface, the expression of transferrin receptor should decrease and, hence, the iron internalization capacity should also decrease. To account for this effect in a model, a relationship between intracellular iron concentration and transferrin receptor expression at cell surface is needed.

Another possible explanation for discrepancy between experiments and simulation is due to the considerations for very large number receptors per cell. A very large number of receptors can facilitate linear transport by providing excess free receptors at the surface of cells. However, the proper selection of receptors per cell was not very easy because for different kind of cells the number of receptors per cell is different. Even for the same kind of cell, different researchers reported different receptor density. For instance, Raub and Newton [19] reported there were 10000 ± 600 receptors/cell, whereas Descamps et al. [21] reported there were 35,000 receptors/cell for bovine brain endothelial cell. As a matter fact, Ciechanover et al. [59] reported even higher (50,000 receptors/cell) for human hepatoma cell line. Nevertheless, presence of large number receptors per cell and/or substantial recruitment of transferrin receptors from intracellular pool to active endocytic pool can prevent saturation of holo-transferrin accumulation even for higher level of hollo-transferrin (1200 ng/ml) at the apical side.

Our model is further validated by comparing with another independent experimental work [21], where 17.5 nM of holo-transferrin initially present on the apical surface of the cells. The transport of holo-transferrin through endothelial cells (from apical side to basolateral side) as a function of time is shown in Fig. 5. An excellent agreement is obtained between the experimental and numerical results. In the experiment [21], re-endocytosis of transferrin via the abluminal compartment was avoided by transferring the cells to another well at various time. Their experimental setup is in line with our model, where we have neglected the re-endocytosis through the abluminal side. Fig. 5 also shows that the transcytosis of holo-transferrin into the brain side is insignificant during the first 15 min of incubation. This time scale indicates the required period for holo-transferrin to cross the BBB endothelial cells.

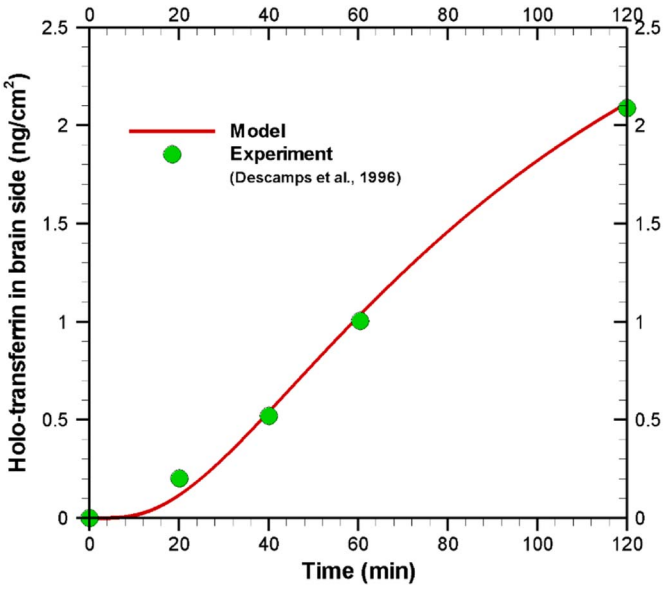

Fig. 5. Holo-transferrin transported to brain side (basolateral side) as a function of time for an initial holo-transferrin concentration of 1400 ng/ml (17.5 nM) in the blood side (apical side). Experimental result from Descamps et al. [21] is shown as green circles, where they cultured their brain capillary endothelial cells with 17.5 nM of holo-transferrin in the apical side.

5.2. Transferrin kinetics and iron transport in cell under normal condition

5.2.1. Recycling vs exocytosis

Next, we study the asymmetric efflux of transferrin from the endothelial cells and compare the results with experimental data [21] at 30 min. In the experiments [21], pulse-chase measurements were made to quantify the possible ligand recycling to the apical side of the cells after endocytosis. To model the experimental observation, we ran the model for 1 h with 1400 ng/ml (17.5 nM) of holo-transferrin in the apical side to mimic the same experimental conditions of Descamps et al. [21]. All the other parameters used during the first 1 h simulation were kept same as in Tables 2 and 3. Then the results are taken as the initial condition for most of the variables except the following compounds: HT_{bl}, AT_{bl}, HT_{br}, Fe_{bl}^{3+} and Fe_{br}^{3+}. The initial values of these variables are set to zero, which is similar to washing of the cells and/or incubating with a new medium in experiments. After that we run the model for 30 more mins using the rate constants given in Table 3. The results predicted by the model are presented in Fig. 6. The percentage of transferrin that goes to the upper or apical compartment (apo-transferrin) is presented with red color line, while the percentage of holo-transferrin that exocytose to lower or basolateral compartment is shown with blue color line and the percentage of holo-transferrin remains inside the cell is presented with magenta color line. Our modeling results indicate that after 30 min 68% of the transferrin is exocytosed to the basolateral side whereas 11% is recycled to the apical side. Our simulation results are consistent with experimental data, where they found that 10% of the transported transferrin was recycled to the apical side, whereas 75% was exocytosed to the basolateral side at 30 mins [21]. However, Raub and Newton [19] found that at 37 °C only 15% of the endocytosed was exocytosed to the basolateral side, whereas 48% of the endocytosed was recycled back to the apical side. The contradicting results from the two experimental studies come from the differences in cell culture conditions and experimental protocols. Former experiment (Descamps et al. [21]) cocultured endothelial cells with astrocytes whereas later experiment took the response of endothelial cells in culture with C_6 glioma cells. The glioma cell reduces the transcytosis across BBB whereas astrocytes may facilitate the transcytosis across BBB [21]. Moreover, former experimentalists worked with post confluent cells (5 days after visualization of the confluence) and they used saponin to gain access to intracellular transferrin receptors pool (90% of the receptors are located in the intracellular receptors pool [60]). As a result, they reported receptor density of 35,000 receptors/cell, which is much higher than the value reported by Raub and Newton [19]. This difference in receptor density indicates that the intracellular iron concentration was different in those two cell preparations because receptor expression depends on the intracellular iron concentration [22]. In our model we have used receptor density of 35,000 receptors/cell, which is similar to the reported value of Descamps et al. [21].

5.2.2. Effect of initial concentration of holo-transferrin on intermediate complexes

Experimental studies have limitations in quantifying various protein complexes that forms during transport of iron across the BBB. For instance, transferrin forms several complexes such holo-transferrin-receptor complex, apo-transferrin-receptor complex etc. at membrane

Table 3
Rate constants used in this study for normal cell.

Rate constants	Definition	Values	Reference
k_1	Association rate of HT and R proteins	$1.7 \times 10^4\,M^{-1}s^{-1}$	[55]
k_{-1}	Dissociation rate of HTR_{as} complex	$1.5 \times 10^{-3}\,s^{-1}$	[25]
k_2	Internalization rate of HTR_{as} complex	$7.5 \times 10^{-3}\,s^{-1}$	[26]
k_3	Dissociation rate of iron from HTR_i complex	$1.125 \times 10^{-3}\,s^{-1}$	[56]
k_4	Rate of recycling of ATR_i complex on surface	$1.08 \times 10^{-3}\,s^{-1}$	[27]
k_5	Dissociation rate of AT from ATR_{as} complex	$4.3 \times 10^{-2}\,s^{-1}$	[25,65]
k_6	Rate of utilization of iron by cells	$0.5 \times 10^{-4}\,s^{-1}$	This work
k_7	Rate of transport of iron across basolateral membrane	$1.8 \times 10^{-4}\,s^{-1}$	This work
k_8	Binding rate of HTR_i and V	$7.5 \times 10^5\,M^{-1}s^{-1}$	This work
k_9	Binding rate of tS with $HTRV_i$ complex	$1.0 \times 10^5\,M^{-1}s^{-1}$	[53,66]
k_{10}	Association rate of S and Syn	$2.0 \times 10^6\,M^{-1}s^{-1}$	[53]
k_{-10}	Dissociation rate of tS	$1.0 \times 10^{-2}\,s^{-1}$	[67]
k_{11}	Rate of dissociation of $HTRVT_{bs}$	$1.15 \times 10^{-3}\,s^{-1}$	This work

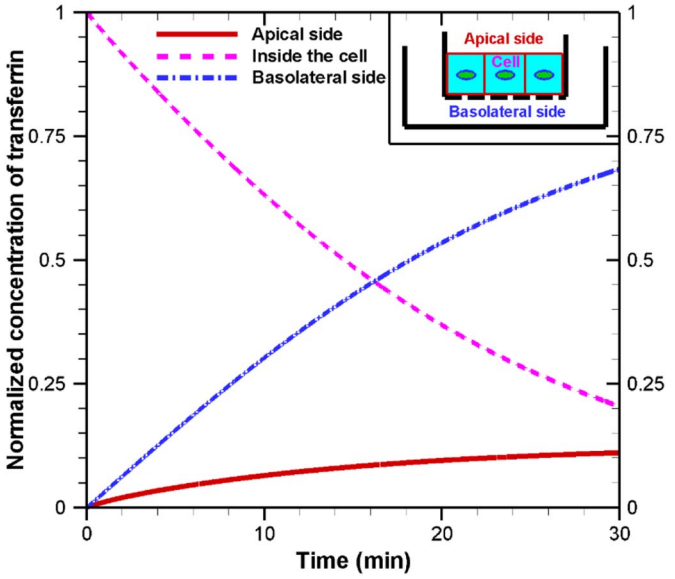

Fig. 6. Temporal distribution of transferrin recycles to apical side, exocytoses to basolateral side and remains inside the endothelial cell. Here all concentrations are normalized with initially endocytosed holo-transferrin amount after first 1 h of incubation. The pulse-chase experiments of Descamps et al. [21] reported that 10% of the transferrin is recycled to the apical side, while 75% of the transferrin is exocytosed to the basolateral side at 30 mins. The concept of apical and basolateral side in a cell culture is shown in inset.

surface and inside the cell by interacting with transferrin receptors and other proteins, which cannot be captured experimentally. However, an appropriately calibrated numerical model can predict the concentration of intermediate complexes at different time points. Here, using our model we study the effect of holo-transferrin concentration in apical side on the transcytosis of irons. For our numerical investigation, we keep all the initial concentrations and rate constants same as in Tables 2 and 3, respectively, and vary the concentration of the holo-transferrin in the apical side. Fig. 7a shows the amount of holo-transferrin internalized by the endothelial cell over a period of 120 min. This internalized transferrin is computed by subtracting the holo-transferrin remaining in blood side from the initial value. As the concentration of holo-transferrin in the blood side increases, the internalized holo-transferrin also increases during the 2 h period. However, as the holo-transferrin concentration increases in the apical side, the percent of internalized holo-transferrin decreases. As shown in Fig. 7a, for 2 nM of holo-transferrin in apical side, 1.71 nM (or 85.5%) of holo-transferrin is internalized by the endothelial cells in 2 h. Whereas, for 40 nM of holo-transferrin in the apical side, 29.52 nM (or 73.8%) of holo-transferrin is internalized in 2 h. Higher percentage of uptake with lower concentration of holo-transferrin is due to the fact that it is easier for ligands to find a free receptor at lower concentration.

The number of free surface receptors remaining on the apical surface of cell is shown in Fig. 7b. As the holo-transferrin concentration increases in the blood side, the number of free receptors on the cell surface decreases. This is due to the fact that with increasing holo-transferrin concentration in blood side, the internalization of transferrin-receptors complex increases, leading to less free receptors. In all cases, the number of free receptors on the cell surface first decreases, reaches minimum at around 20 min, and then increases. This is due to the fact that the internalization rate is much higher compared to exocytosis rate at the beginning. After 20 min, the exocytosis of holo-transferrin to brain side increases and the internalized receptors recycle back to the apical surface, which increases the number of free receptors at the surface. Fig. 7b also indicates that even with 40 nM of holo-transferrin, there is a large number of free receptors on the apical surface. This result also explains why the accumulation of holo-transferrin is not saturated even at high concentrations of holo-transferrin in the apical side (Fig. 4).

As the ligand concentration increases, the internalization also increases (Fig. 7a). This results in a sharp increase in both recycling of apo-transferrin (Fig. 7c) and transcytosis of holo-transferrin (Fig. 7d). Fig. 7(c) and (d) also show that during the first ~20 min, the recycling and transcytosis of transferrin are almost undetectable. This indicates the time needed for recycling or transcytosis of transferrin through BBB endothelial cells. The predicted cycling time is comparable with other type of cells such as human hepatoma cell [25] and human choriocarcinoma cell [61].

5.3. Transferrin kinetics and iron transport in iron-enriched and iron-depleted cell

According to the World Health Organization (WHO), serum ferritin concentrations of < 15 μg/l indicate depleted iron states, whereas serum ferritin concentrations > 200 μg/l suggest severe risk of iron overload [62]. The intracellular iron concentration is generally related to the plasma iron level, which controls the surface receptors for transferrin binding at the apical side. Descamps et al. [21] reported 35,000 receptors for a normal endothelial cell. But this number will be higher and lower for the iron-depleted and iron-enriched cells. For our model, we have estimated the surface receptor density based on the existing experimental findings. Gelder et al. [58] experimentally quantified the number of transferrin binding sites per mg of transferrin receptors for iron-depleted and iron-enriched cells as 2.79×10^{11} and 2.25×10^{11}respectively. Literatures also suggest that each cell might contain 8.3×10^{-8} [19] to 2.5×10^{-7} [25] mg of transferrin receptors. If we consider 1.425×10^{-7} mg of transferrin receptors per cell, the corresponding surface receptors (per cell) become 39,857 and 32,143 for iron-depleted and iron-enriched cell, respectively. We use these values of transferrin receptors per cell for iron-depleted and iron-

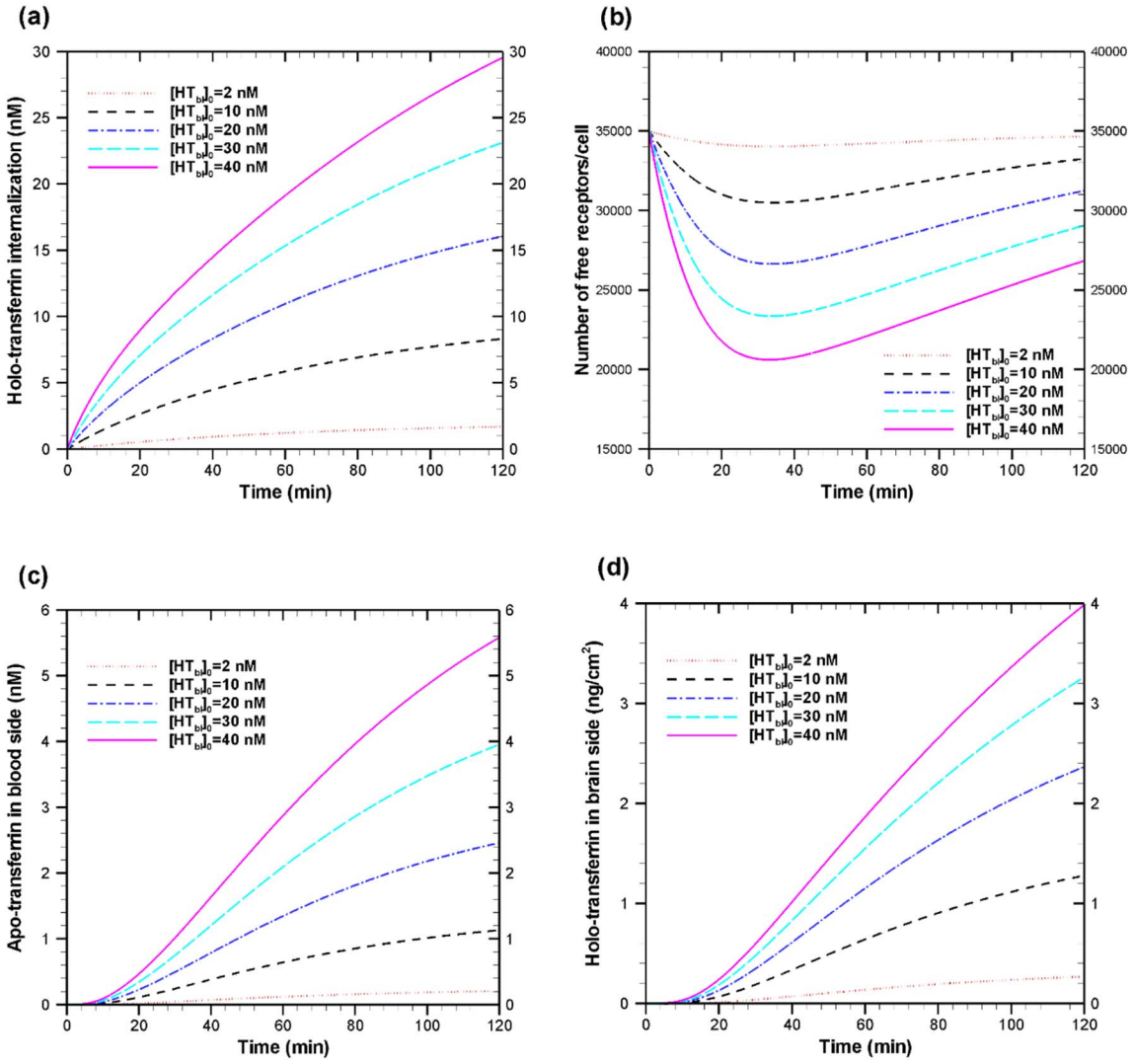

Fig. 7. Effect of ligand (holo-transferrin) concentration variation on (a) holo-transferrin internalization through the apical side, (b) number of surface receptors (free) per cell on apical surface, (c) recycled apo-transferrin concentration in the apical side and, (d) amount of holo-transferrin transported to the basolateral side. Related rate constants and initial concentrations of presented in Tables 2 and 3.

Table 4
Rate constants used in this study for iron-depleted and iron-enriched cells.

Rate constants	Cell types		Reference
	Iron-depleted cell	Iron-enriched cell	
k_1	$1.7 \times 10^4\,M^{-1}s^{-1}$	$1.7 \times 10^4\,M^{-1}s^{-1}$	[55]
k_{-1}	$1.5 \times 10^{-3}\,s^{-1}$	$1.5 \times 10^{-3}\,s^{-1}$	[25]
k_2	$4.8 \times 10^{-3}\,s^{-1}$	$10.5 \times 10^{-3}\,s^{-1}$	[58]
k_3	$3.9 \times 10^{-3}\,s^{-1}$	$2.25 \times 10^{-4}\,s^{-1}$	This work
k_4	$1.1 \times 10^{-3}\,s^{-1}$	$8.5 \times 10^{-4}\,s^{-1}$	[58]
k_5	$4.3 \times 10^{-2}\,s^{-1}$	$4.3 \times 10^{-2}\,s^{-1}$	[25,65]
k_6	$5.0 \times 10^{-4}\,s^{-1}$	$0.5 \times 10^{-4}\,s^{-1}$	This work
k_7	$1.8 \times 10^{-5}\,s^{-1}$	$1.8 \times 10^{-5}\,s^{-1}$	This work
k_8	$7.5 \times 10^5\,M^{-1}s^{-1}$	$7.5 \times 10^5\,M^{-1}s^{-1}$	This work
k_9	$1.0 \times 10^5\,M^{-1}s^{-1}$	$1.0 \times 10^5\,M^{-1}s^{-1}$	[53,66]
k_{10}	$2.0 \times 10^6\,M^{-1}s^{-1}$	$2.0 \times 10^6\,M^{-1}s^{-1}$	[53]
k_{-10}	$1.0 \times 10^{-2}\,s^{-1}$	$1.0 \times 10^{-2}\,s^{-1}$	[67]
k_{11}	$1.15 \times 10^{-3}\,s^{-1}$	$1.15 \times 10^{-3}\,s^{-1}$	This work

enriched cells, respectively. These values are consistent with the experimental works of Descamps et al. [21].

To predict the iron transport for iron-depleted and iron-enriched cells, we also need to re-adjust some of the kinetic rate constants. The internalization rate constant, k_2 is changed for iron-depleted and iron-enriched cells according to the work of Gelder et al. [58]. They determined the half-life of internalization as 2.3 min (k_2 = 0.3 min^{-1}) and 1.1 min (k_2 = 0.62 min^{-1}) for iron-depleted and iron-enriched cultured cells, respectively. They also determined the half-life of exocytosis for transferrin recycling as 11.6 min (k_{out} = 0.06 min^{-1}) and 14.6 min (k_{out} = 0.05 min^{-1}) for iron-depleted and iron-enriched cultured cells, respectively.

The dissociation rate of apo-transferrin from apo-transferrin-receptor complex, k_5 depends on the pH of the apical medium solution. Thus, we consider the value of k_5 the same as normal cell. From $1/k_{out} = 1/k_4 + 1/k_5$, we determine the rate of recycling of apo-transferrin-receptor complex, k_4 on the apical surface. Finally, we have modified the acidification rate, k_3 for iron enriched and iron depleted cell. Since iron-enriched cells already have sufficient irons, acidification in the endosomal compartment is greatly reduced. On the other hand, iron-depleted cells are suffering from iron deficiency, so they need more irons to regain the normal functions. As a result, a high acidification rate in the endosomal compartment is necessary in iron-depleted cells. Here, we determine the acidification rates for both iron-enriched and iron-depleted cell by comparing the model output with the experimental results of Burdo et al. [22]. The rate constants used for iron transport in iron-depleted cell and iron-enriched cell are given in

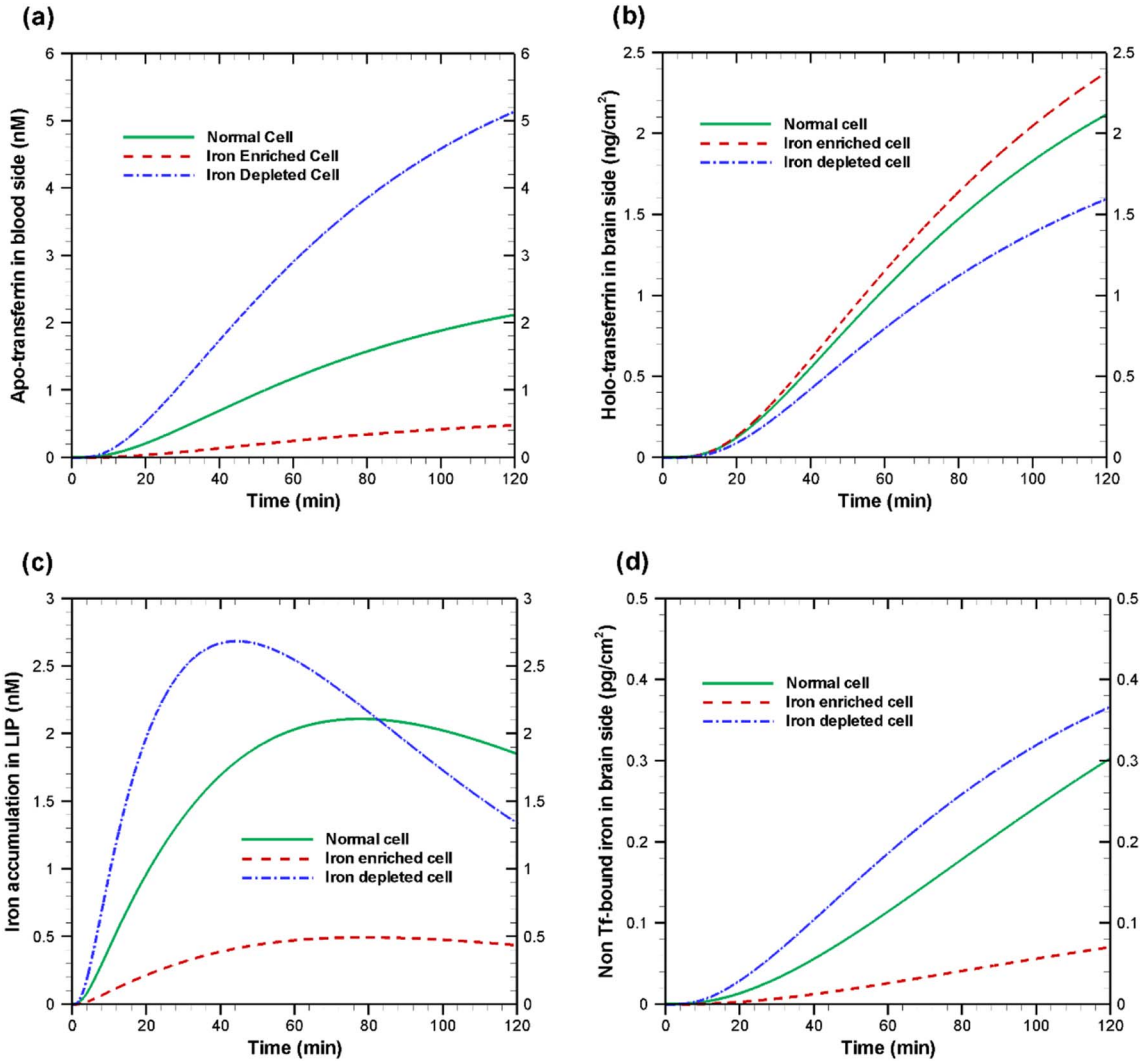

Fig. 8. Comparison of transport processes among normal, iron-enriched and iron-depleted cells. Concentration of a) apo-transferrin recycled back to blood side, b) holo-transferrin transported to brain side, c) (free) iron accumulated in LIP and d) free iron transported to brain side. In all cases, the cell is incubated with 17.5 nM of holo-transferrin in apical side for 2 h.

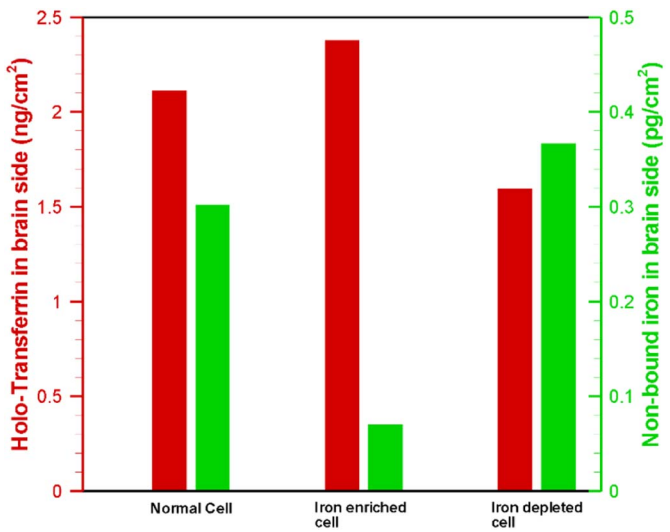

Fig. 9. Bar chart showing transferrin bound (holo-transferrin) and free iron transport in the brain side. All simulation conditions are same as in Fig. 8.

Table 4, whereas for normal cell all rate constants are the same as listed in Table 3. The initial concentrations are kept the same as normal cell (Table 2) except the number of receptors/cell.

Various forms of iron and transferrin concentrations are shown in Fig. 8 for normal, iron-depleted and iron-overloaded endothelial cells during 2 h of incubation with 17.5 nM of holo-transferrin in the apical sides. Fig. 8(a) indicates that in comparison to normal cell, the iron-depleted cell has higher amount of apo-transferrin recycling to blood side whereas iron-enriched cell has lower amount of recycling of apo-transferrin. Since the iron-depleted cell needs more irons than iron-enriched cell to maintain the proper cell functioning, the acidification rate in endosomal compartment is higher for iron-depleted cell than iron-enriched cell [22]. This leads to higher amount of apo-transferrin recycling in iron-depleted case. However, to meet the brain needs of iron and transferrin, the transferrin-bound iron is not significantly changed in different types of cells (see Fig. 8(b)). On the other hand, due to low acidification rate in endosome, in an iron-enriched cell, the non-transferrin bound iron is greatly reduced in the brain side (see Fig. 8(d)). The accumulation rate of free irons in the LIP is shown in Fig. 8(c). Due to high acidification rate of holo-transferrin in iron-depleted cell, the irons accumulate quickly during the first hour, and then the accumulation decreases to meet the high demand of irons in mitochondria and other cytoplasmic iron-dependent organelles. For iron-

Table 5
Comparison of model results with experimental observations for iron-enriched and iron-depleted cell. Results are presented for percentage change in iron concentration with respect to normal cell.

Cell type	Transferrin-bound iron in brain side		Free iron in brain side	
	Iron-enriched	Iron-depleted	Iron-enriched	Iron-depleted
Experiment[a]	+15.7%	−25.7%	−73.5%	+19.2%
Model	+13.9%	−24.5%	−76.7%	+21.3%

Note: A negative sign indicates reduction whereas a positive sign indicates increase with respect to normal cell.

[a] Experimental values are calculated from the data provided in reference [22].

enriched cell, a low iron accumulation is observed throughout the 2 h period.

Fig. 9 shows the bar chart of transferrin-bound (holo-transferrin) and non-transferrin bound (free) iron for three different cell types after 2 h incubation with 17.5 nM of holo-transferrin in the apical side. For normal cell, 2.1 ng/cm^2 of holo-transferrin is transported to the brain side by the endothelial cells. Since 1 g holo-transferrins contain 1.375 mg of iron, there are 2.9 pg/cm^2 of irons transported as bound to transferrin, and only 0.32 pg/cm^2 iron is transported to brain side as free iron. In other words, 10% of total irons are transported to the brain side as ion and the rest are transported as transferrin-bound iron. The free iron transported to the brain side becomes 2% and 14% for iron-enriched and iron-depleted cell, respectively. The changes in iron transport (both as free and transferrin-bound) from the normal cell condition are shown in Table 5 for iron-depleted and iron-enriched cell. Our model shows that there is nearly 75% decrease in free iron in iron-rich cell, while there is approximately 20% increase in free iron in iron-depleted cells. These changes in iron contents qualitatively agree with experimental observations of Brudo et al. [22].

6. Conclusions

A comprehensive mathematical model is developed for kinetics of transferrin endocytosis, recycling, and exocytosis during the iron transport through the BBB endothelial cells. The model takes into account two possible pathways of iron transport from blood to brain in an in-vitro scenario. Unknown kinetic parameters are determined by a non-linear optimization technique by comparing our model prediction with experimental data. Based on the estimated rate constants, our model was able to predict the iron and transferrin transport behavior in a number of in vitro scenarios. Like any parameter estimation process, our predicted rate constants are valid for the specific scenarios presented and assumptions used.

We have shown that our model can be used to predict the time-dependent asymmetric efflux of transferrin through apical and basolateral surface of brain capillary endothelial cells. Although some experimental observations suggest saturation of transferrin accumulation inside the endothelial cell for higher holo-transferrin concentration (> 10 nM) in the blood, this transferrin saturation can be prevented by altering the receptor expression. Transferrin accumulation inside the cell can also be enhanced by recruiting transferrin receptors from intracellular pool to active endocytic pool.

Our pathway based model was used to predict the concentration of various compounds at different compartments during the transport of iron through BBB endothelial cells. Our results indicate that, for a healthy cell, iron transport rate through brain side increases with increasing holo-transferrin concentration in the blood side. A similar finding is obtained for recycling of apo-transferrin with change in holo-transferrin concentration in the blood side.

We also studied the iron transport mechanism in iron-rich and iron-deficient cells. Our results indicate that the cell iron status controls the acidification rate in the endosome and determines the extent of two possible iron transport pathways in BBB endothelium. Model results also suggest that the free iron transport to the brain side significantly reduced in iron-enriched cell, whereas, a slightly increased free iron transport is predicted in an iron-depleted cell. Our numerical results also show that due to high utilization of the iron in iron-depleted cell, a large quantity of irons are not transported in the brain side although there is a high acidification rate in the endosome. The rate of transferrin recycled to the blood side is higher for iron-depleted cell compare to iron-enriched cell. This results in a higher iron accumulation in LIP for iron-deficient cells.

Transparency document

The http://dx.doi.org/10.1016/j.bbagen.2018.02.010 associated with this article can be found, in online version.

Acknowledgement

This work was supported by the National Institute of General Medical Sciences of the National Institutes of Health under Award Number R01GM122081. The content is solely the responsibility of the authors and does not necessarily represent the official views of the National Institutes of Health.

References

[1] N.J. Abbott, Dynamics of CNS barriers: evolution, differentiation, and modulation, Cell. Mol. Neurobiol. 25 (1) (2005) 5–23.
[2] N.J. Abbott, A.A. Patabendige, D.E. Dolman, S.R. Yusof, D.J. Begley, Structure and function of the blood–brain barrier, Neurobiol. Dis. 37 (1) (2010) 13–25.
[3] U. Kniesel, H. Wolburg, Tight junctions of the blood–brain barrier, Cell. Mol. Neurobiol. 20 (1) (2000) 57–76.
[4] C. Schulze, J.A. Firth, Immunohistochemical localization of adherens junction components in blood-brain-barrier microvessels of the rat, J. Cell Sci. 104 (1993) 773–782.
[5] H.E. de Vries, J. Kuiper, A.G. de Boer, T.J. Van Berkel, D.D. Breimer, The blood-brain barrier in neuroinflammatory diseases, Pharmacol. Rev. 49 (2) (1997) 143–156.
[6] B.T. Hawkins, T.P. Davis, The blood-brain barrier/neurovascular unit in health and disease, Pharmacol. Rev. 57 (2) (2005) 173–185.
[7] W.M. Pardridge, Molecular Trojan horses for blood–brain barrier drug delivery, Curr. Opin. Pharmacol. 6 (5) (2006) 494–500.
[8] D. Berg, H. Hochstrasser, Iron metabolism in parkinsonian syndromes, Mov. Disord. 21 (9) (2006) 1299–1310.
[9] H. Jiang, J. Wang, J. Rogers, J. Xie, Brain iron metabolism dysfunction in Parkinson's disease, Mol. Neurobiol. (2016) 1–24.
[10] W.-Y. Ong, A.A. Farooqui, Iron, neuroinflammation, and Alzheimer's disease, J. Alzheimers Dis. 8 (2) (2005) 183–200.
[11] J.H. Jandl, J.K. Inman, R.L. Simmons, D.W. Allen, Transfer of iron from serum iron-binding protein to human reticulocytes, J. Clin. Investig. 38 (1 Pt. 1–2) (1959) 161.
[12] F.M. van Bockxmeer, E. Morgan, Identification of transferrin receptors in reticulocytes, Biochim. Biophys. Acta Biomembr. 468 (3) (1977) 437–450.
[13] T.A. Hamilton, H.G. Wada, H.H. Sussman, Identification of transferrin receptors on the surface of human cultured cells, Proc. Natl. Acad. Sci. 76 (12) (1979) 6406–6410.
[14] P.A. Seligman, R.B. Schleicher, R.H. Allen, Isolation and characterization of the transferrin receptor from human placenta, J. Biol. Chem. 254 (20) (1979) 9943–9946.
[15] W.P. Faulk, B.-L. Hsi, P. Stevens, Transferrin and transferrin receptors in carcinoma of the breast, Lancet 316 (8191) (1980) 390–392.
[16] W.A. Jefferies, M.R. Brandon, S.V. Hunt, A.F. Williams, K.C. Gatter, D.Y. Mason, Transferrin receptor on endothelium of brain capillaries, Nature 312 (5990) (1984) 162–163.
[17] J. Fishman, J. Rubin, J. Handrahan, J. Connor, R. Fine, Receptor-mediated transcytosis of transferrin across the blood-brain barrier, J. Neurosci. Res. 18 (2) (1987) 299–304.
[18] E.M. Taylor, E.H. Morgan, Developmental changes in transferrin and iron uptake by the brain in the rat, Dev. Brain Res. 55 (1) (1990) 35–42.
[19] T.J. Raub, C.R. Newton, Recycling kinetics and transcytosis of transferrin in primary cultures of bovine brain microvessel endothelial cells, J. Cell. Physiol. 149 (1) (1991) 141–151.
[20] C. Morris, A. Keith, J. Edwardson, R. Pullen, Uptake and distribution of iron and transferrin in the adult rat brain, J. Neurochem. 59 (1) (1992) 300–306.
[21] L. Descamps, M.-P. Dehouck, G. Torpier, R. Cecchelli, Receptor-mediated transcytosis of transferrin through blood-brain barrier endothelial cells, Am. J. Phys. Heart Circ. Phys. 270 (4) (1996) H1149–H1158.

[22] J.R. Burdo, D.A. Antonetti, E.B. Wolpert, J.R. Connor, Mechanisms and regulation of transferrin and iron transport in a model blood-brain barrier system, Neuroscience 121 (4) (2003) 883–890.

[23] M. Hersom, H.C. Helms, N. Pretzer, C. Goldeman, A.I. Jensen, G. Severin, M.S. Nielsen, R. Holm, B. Brodin, Transferrin receptor expression and role in transendothelial transport of transferrin in cultured brain endothelial monolayers, Mol. Cell. Neurosci. 76 (2016) 59–67.

[24] T.A. Rouault, S. Cooperman, "Brain iron metabolism,", Proc. Seminars in Pediatric Neurology 13 (3) (2006) 142–148 Elsevier.

[25] A. Ciechanover, A. Schwartz, A. Dautry-Varsat, H. Lodish, Kinetics of internalization and recycling of transferrin and the transferrin receptor in a human hepatoma cell line. Effect of lysosomotropic agents, J. Biol. Chem. 258 (16) (1983) 9681–9689.

[26] B.J. Iacopetta, E.H. Morgan, The kinetics of transferrin endocytosis and iron uptake from transferrin in rabbit reticulocytes, J. Biol. Chem. 258 (15) (1983) 9108–9115.

[27] N. Gironès, R.J. Davis, Comparison of the kinetics of cycling of the transferrin receptor in the presence or absence of bound diferric transferrin, Biochem. J. 264 (1) (1989) 35–46.

[28] Y. Shitara, Y. Kato, Y. Sugiyama, Effect of brefeldin A and lysosomotropic reagents on intracellular trafficking of epidermal growth factor and transferrin in Madin-Darby canine kidney epithelial cells, J. Control. Release 55 (1) (1998) 35–43.

[29] K.M. Mayle, A.M. Le, D.T. Kamei, The intracellular trafficking pathway of transferrin, Biochim. Biophys. Acta Gen. Subj. 1820 (3) (2012) 264–281.

[30] D.F. Leitner, J.R. Connor, Functional roles of transferrin in the brain, Biochim. Biophys. Acta Gen. Subj. 1820 (3) (2012) 393–402.

[31] R. Roberts, A. Sandra, G. Siek, J. Lucas, R. Fine, Studies of the mechanism of iron transport across the blood-brain barrier, Ann. Neurol. 32 (S1) (1992) S43–S50.

[32] S. Skarlatos, T. Yoshikawa, W.M. Pardridge, Transport of [125 I] transferrin through the rat blood-brain barrier, Brain Res. 683 (2) (1995) 164–171.

[33] S. Parkkila, A. Waheed, R.S. Britton, B.R. Bacon, X.Y. Zhou, S. Tomatsu, R.E. Fleming, W.S. Sly, Association of the transferrin receptor in human placenta with HFE, the protein defective in hereditary hemochromatosis, Proc. Natl. Acad. Sci. U. S. A. 94 (24) (1997) 13198–13202.

[34] T.R. Daniels, T. Delgado, J.A. Rodriguez, G. Helguera, M.L. Penichet, The transferrin receptor part I: biology and targeting with cytotoxic antibodies for the treatment of cancer, Clin. Immunol. 121 (2) (2006) 144–158.

[35] A. Calzolari, L.M. Larocca, S. Deaglio, V. Finisguerra, A. Boe, C. Raggi, L. Ricci-Vitani, F. Pierconti, F. Malavasi, R. De Maria, Transferrin receptor 2 is frequently and highly expressed in glioblastomas, Transl. Oncol. 3 (2) (2010) 123–134.

[36] A. Dautry-Varsat, A. Ciechanover, H.F. Lodish, pH and the recycling of transferrin during receptor-mediated endocytosis, Proc. Natl. Acad. Sci. 80 (8) (1983) 2258–2262.

[37] B.M. Pearse, M.S. Robinson, Clathrin, adaptors, and sorting, Annu. Rev. Cell Biol. 6 (1) (1990) 151–171.

[38] D.J. Yamashiro, F.R. Maxfield, Acidification of endocytic compartments and the intracellular pathways of ligands and receptors, J. Cell. Biochem. 26 (4) (1984) 231–246.

[39] H. Gunshin, B. Mackenzie, U.V. Berger, Y. Gunshin, M.F. Romero, W.F. Boron, S. Nussberger, J.L. Gollan, M.A. Hediger, Cloning and characterization of a mammalian proton-coupled metal-ion transporter, Nature 388 (6641) (1997) 482–488.

[40] M.W. Hentze, M.U. Muckenthaler, B. Galy, C. Camaschella, Two to tango: regulation of mammalian iron metabolism, Cell 142 (1) (2010) 24–38.

[41] B.D. Grant, J.G. Donaldson, Pathways and mechanisms of endocytic recycling, Nat. Rev. Mol. Cell Biol. 10 (9) (2009) 597–608.

[42] E. Mills, X.P. Dong, F.D. Wang, H.X. Xu, Mechanisms of brain iron transport: insight into neurodegeneration and CNS disorders, Future Med. Chem. 2 (1) (2010) 51–64.

[43] S.A. Predescu, D.N. Predescu, K. Shimizu, I.K. Klein, A.B. Malik, Cholesterol-dependent syntaxin-4 and SNAP-23 clustering regulates caveolar fusion with the endothelial plasma membrane, J. Biol. Chem. 280 (44) (2005) 37130–37138.

[44] S.E. Holstein, H. Ungewickell, E. Ungewickell, Mechanism of clathrin basket dissociation: separate functions of protein domains of the DnaJ homologue auxilin, J. Cell Biol. 135 (1996) 925–937.

[45] M.W. Hentze, M.U. Muckenthaler, N.C. Andrews, Balancing acts: molecular control of mammalian iron metabolism, Cell 117 (3) (2004) 285–297.

[46] S. Rodrigues, M. Desroches, M. Krupa, J.M. Cortes, T.J. Sejnowski, A.B. Ali, Time-coded neurotransmitter release at excitatory and inhibitory synapses, Proc. Natl. Acad. Sci. U. S. A. 113 (8) (2016) E1108–E1115.

[47] I.R. Pulido, R. Jahn, V. Gerke, VAMP3 is associated with endothelial Weibel-Palade bodies and participates in their Ca2+-dependent exocytosis, BBA-Mol. Cell. Res. 1813 (5) (2011) 1038–1044.

[48] Q.Y. Zhu, M. Yamakuchi, C.J. Lowenstein, SNAP23 regulates endothelial exocytosis of von Willebrand factor, PLoS One 10 (8) (2015).

[49] M. Schillemans, D. van Breevoort, M. Hofman, M. Wahedi, A. Gangaev, H. Meems, M. van den Biggelaar, R. Adam, H. Janssen, S. Meijer, J. Voorberg, R. Bierings, Regulation of weibel-palade body exocytosis from endothelial cells by syntaxin-3 and stxbp5 containing snare complexes, Haematologica 101 (2016) 312–313.

[50] S.H. Low, S.J. Chapin, T. Weimbs, L.G. Komuves, M.K. Bennett, K.E. Mostov, Differential localization of syntaxin isoforms in polarized Madin-Darby canine kidney cells, Mol. Biol. Cell 7 (12) (1996) 2007–2018.

[51] C.R. Vogel, Computational Methods for Inverse Problems, SIAM, 2002.

[52] L. Gilles, C. Vogel, J. Bardsley, Computational methods for a large-scale inverse problem arising in atmospheric optics, Inverse Prob. 18 (1) (2002) 237.

[53] W. Chen, W. Zhou, T. Xia, X. Gu, A computational analysis framework for molecular cell dynamics: case-study of exocytosis, PLoS One 7 (7) (2012) e38699.

[54] R.J. Ritchie, T. Prvan, Current statistical methods for estimating the K_m and V_{max} of Michaelis-Menten kinetics, Biochem. Educ. 24 (4) (1996) 196–206.

[55] J. Sainte-Marie, M. Vidal, P. Bette-Bobillo, J.R. Philippot, A. Bienvenüe, The influence of transferin binding to L2C guinea pig leukemic lymphocytes on the endocytosis cycle kinetics of its receptor, FEBS J. 201 (1) (1991) 295–302.

[56] J.A. Lebron, M.J. Bennett, D.E. Vaughn, A.J. Chirino, P.M. Snow, G.A. Mintier, J.N. Feder, P.J. Bjorkman, Crystal structure of the hemochromatosis protein HFE and characterization of its interaction with transferrin receptor, Cell 93 (1) (1998) 111–123.

[57] C.C. Visser, L.H. Voorwinden, D.J.A. Crommelin, M. Danhof, A.G. de Boer, Characterization and modulation of the transferrin receptor on brain capillary endothelial cells, Pharm. Res. 21 (5) (2004) 761–769.

[58] W. van Gelder, M.I.E. Huijskes-Heins, M.I. Cleton-Soeteman, J.P. van Dijk, H.G. van Eijk, Iron uptake in blood-brain barrier endothelial cells cultured in iron-depleted and iron-enriched media, J. Neurochem. 71 (3) (1998) 1134–1140.

[59] A. Ciechanover, A.L. Schwartz, H.F. Lodish, The asialoglycoprotein receptor internalizes and recycles independently of the transferrin and insulin-receptors, Cell 32 (1) (1983) 267–275.

[60] W. Vangelder, M.I.E. Huijskesheins, J.P. Vandijk, M.I. Cletonsoeteman, H.G. Vaneijk, Quantification of different transferrin receptor pools in primary cultures of porcine blood-brain-barrier endothelial-cells, J. Neurochem. 64 (6) (1995) 2708–2715.

[61] A. van der Ende, A. du Maine, A.L. Schwartz, G.J. Strous, Modulation of transferrin-receptor activity and recycling after induced differentiation of BeWo choriocarcinoma cells, Biochem. J. 270 (2) (1990) 451–457.

[62] W.H. Organization, Serum Ferritin Concentrations for the Assessment of Iron Status and Iron Deficiency in Populations, (2011).

[63] A. Mezer, E. Nachliel, M. Gutman, U. Ashery, A new platform to study the molecular mechanisms of exocytosis, J. Neurosci. 24 (40) (2004) 8838–8846.

[64] H. Fujita, P.L. Tuma, C.M. Finnegan, L. Locco, A.L. Hubbard, Endogenous syntaxins 2, 3 and 4 exhibit distinct but overlapping patterns of expression at the hepatocyte plasma membrane, Biochem. J. 329 (1998) 527–538.

[65] R.J. Davis, M. Faucher, L.K. Racaniello, A. Carruthers, M.P. Czech, Insulin-like growth factor-i and epidermal growth-factor regulate the expression of transferrin receptors at the cell-surface by distinct mechanisms, J. Biol. Chem. 262 (27) (1987) 13126–13134.

[66] D. Fasshauer, M. Margittai, A transient N-terminal interaction of SNAP-25 and syntaxin nucleates SNARE assembly, J. Biol. Chem. 279 (9) (2004) 7613–7621.

[67] A.V. Pobbati, A. Stein, D. Fasshauer, N- to C-terminal SNARE complex assembly promotes rapid membrane fusion, Science 313 (5787) (2006) 673–676.

[68] B. Garipcan, S. Maenz, T. Pham, U. Settmacher, K.D. Jandt, J. Zanow, J. Bossert, Image analysis of endothelial microstructure and endothelial cell dimensions of human arteries–a preliminary study, Adv. Eng. Mater. 13 (1–2) (2011) B54–B57.